Univerzita Karlova v Praze
Matematicko-fyzikální fakulta

Autoreferát dizertační práce

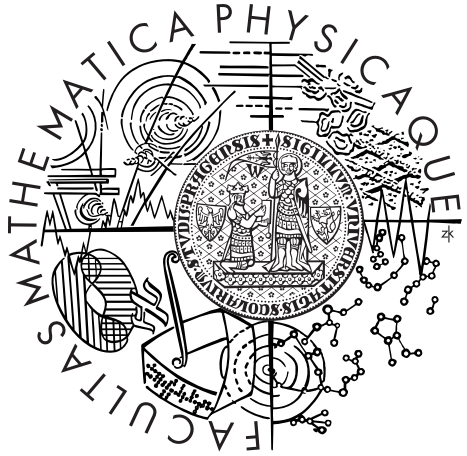

Eliška Zábranová

Modelování vlastních kmitů Země použité na data ze supravodivých gravimetrů v nízkofrekvenční seismické oblasti

Katedra geofyziky

Vedoucí dizertační práce: Doc. RNDr. Ctirad Matyska, DrSc.

Studijní program: Fyzika

Studijní obor: Geofyzika

Praha 2015

Charles University in Prague
Faculty of Mathematics and Physics

Summary of doctoral thesis

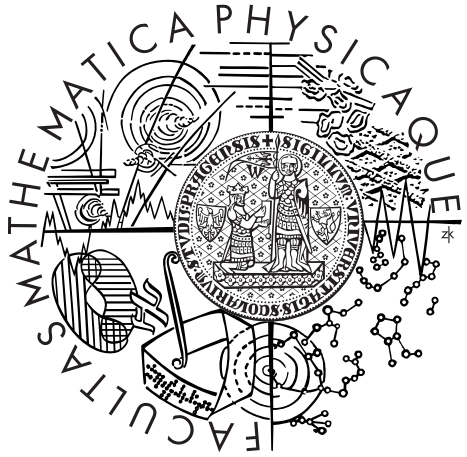

Eliška Zábranová

Numerical modeling of free oscillations applied to superconducting-gravimeter data in a low-frequency seismic range

Department of Geophysics

Supervisor of the doctoral thesis: Doc. RNDr. Ctirad Matyska, DrSc.

Study programme: Physics

Specialization: Geophysics

Prague 2015

Dizertace byla vypracována na základě výsledků získaných v letech 2008–2015 během doktorandského studia na Katedře geofyziky MFF UK.

Dizertant:
RNDr. Eliška Zábranová
Katedra geofyziky MFF UK
V Holešovičkách 2, 180 00 Praha 8

Školitel:
Doc. RNDr. Ctirad Matyska, DrSc.
Katedra geofyziky MFF UK
V Holešovičkách 2, 180 00 Praha 8

Oponenti:
Prof. RNDr. Zdeněk Martinec, DrSc.
Dublin Institute for Advanced Studies
5 Merrion Square, Dublin 2, Ireland
Katedra geofyziky MFF UK
V Holešovičkách 2, 180 00 Praha 8

RNDr. Václav Vavryčuk, DrSc.
Geofyzikální ústav Akademie věd ČR, v.v.i.
Boční II 1401, 141 31 Praha 4

Předseda oborové rady:
Doc. RNDr. Hana Čížková, Ph.D.
Katedra geofyziky MFF UK
V Holešovičkách 2, 180 00 Praha 8

Autoreferát byl rozeslán dne

Obhajoba dizertace se koná dne 14. 9. 2015 v 10 hodin před komisí pro obhajoby dizertačních prací v oboru Geofyzika v budově MFF UK, Ke Karlovu 3, Praha 2, v místnosti č. 105.

S dizertací je možno se seznámit v PGS MFF UK, Ke Karlovu 3, Praha 2.

Contents

Introduction

Normal modes or free oscillations are components of standing waves with an infinite number of degrees of freedom that are created from the constructive interference of body and surface waves circling the Earth multiple times. For the commonly used spherically symmetric, non-rotating, perfectly elastic and isotropic (SNREI) Earth model the oscillations are composed of two distinct types of modes. The spheroidal modes ${}_nS_l$ correspond to standing Rayleigh waves and change the external shape and internal density of the body, and the toroidal modes ${}_nT_l$ correspond to standing Love waves with purely tangential displacements and leave the shape and the radial density distribution unaffected. The modes are labelled by the angular degree $l = 0, \ldots, \infty$ of spherical harmonic decomposition and the prefix overtone number $n = 0, \ldots, \infty$ since there is an infinite number of spheroidal and toroidal modes with angular frequencies ${}_n\omega_l^{\mathrm{S}}$ and ${}_n\omega_l^{\mathrm{T}}$ for a given value of l. In the case of a SNREI model, each of the ${}_nS_l$ and ${}_nT_l$ modes represents a multiplet containing $2l + 1$ oscillations of the same frequency. This $2l + 1$ degeneracy is a mathematical consequence of the model spherical symmetry. When a slightly anelastic model is considered, each multiplet is attenuated with time; the exponential decrease of modal amplitudes is described by quality factors.

Free oscillations provide information about both the internal structure of the Earth and the mechanism of a source event (earthquake, impact etc.) since the periods of the modes are given by model parameters and the amplitudes depend on the source event. The periods of about one thousand normal modes and about one hundred normal-mode quality-factor values were used in addition to travel time observations in constructing the Preliminary Reference Earth Model (Dziewonski and Anderson, 1981) that still represents the fundamental spherically symmetric seismic model of the Earth. Free oscillations also become important in constraining the seismic-source properties of very large earthquakes where the frequency content of the source processes shifts to lower frequencies and determination of seismic moment using high-frequency data becomes problematic. The 2004 Sumatra-Andaman earthquake is a recent example where the standard seismological routines based on the body and surface waves (with periods of several hundred seconds) undervalued the energy released during the rupture process. On the basis of the free-oscillations

analysis Park et al. (2005) showed that the seismic scalar moment M_0 was at least 1.5 times higher than the value inferred from the Global Centroid Moment Tensor (GCMT) solution based on routine procedures.

The traditional approach of computing eigenfrequencies and eigenfunctions of the SNREI model is based on the Runge-Kutta numerical integration of six (two) ordinary differential equations of the first order in the case of spheroidal (toroidal) oscillations. We have developed a different approach where the direct numerical discretization of the ordinary differential equations by high-accuracy pseudospectral schemes (Fornberg, 1996) leads to a series of matrix eigenvalue problems for evaluating eigenfrequencies and eigenfunctions (Zábranová et al., 2009). Our method is a modification of Hanyk et al. (2002) where similar ordinary differential equations are solved for postglacial rebound. In order to check our results, we use the Mineos software package.

The network of superconducting gravimeters (SG) was created to observe seismic normal modes, the Slichter triplet, tidal gravity, ocean tidal loading, core nutations and core modes within the framework of the Global Geodynamics Project (GGP), an international program of observations of temporal variations in the Earth gravity field (Crossley et al., 1999). While older studies have shown that the SGs were not as good as the STS-1 seismometers in the seismic band (Freybourger et al., 1997; Van Camp, 1999), the new generation of SG instruments achieved lower noise levels than any other sensor at frequencies below 0.8 mHz (Widmer-Schnidrig, 2003). Observations of fundamental low-frequency modes are of excellent quality and new SG data enable us to solve a variety of other problems. In this thesis we chose the SG records of the 2010 Maule, 2011 Tohoku and 2012 Sumatra earthquakes in the frequency range below 1 mHz. Since source durations of these earthquakes are shorter than 200 s and the characteristic rupture lengths are smaller than 500 km, we can securely use the point-source approximation in this frequency range.

As we know from the normal-mode perturbation theory (e.g., Backus and Gilbert, 1961; Dahlen, 1968; Dziewonski and Sailor, 1976; Woodhouse and Dahlen, 1978), the free oscillations of the Earth are split by rotation, ellipticity and lateral heterogeneity. In applications to source-mechanism problems we follow the study by Dahlen and Sailor (1979). Splitting of the low-frequency modes is almost insensible to the 3-D structure of the Earth (e.g., He and Tromp, 1996). The new observations of the gravest spheroidal modes by SGs can thus be modelled straightforwardly by taking into account multiplet splitting due to only rotation and ellipticity. These observations yield constraints that can be used to obtain low-frequency limits of the source mechanism together with new estimates of the quality factors of these modes, which we discuss in detail in the second part of this thesis. We also focused on the radial modes ${}_0S_0$ and ${}_1S_0$. Since they are not degenerated, their quality factors can be directly determined from records and the moment tensor inversion can be performed separately.

1 Computational methods

The complete system of PDEs for the Lagrangian displacement $\boldsymbol{u}$, the Eulerian incremental gravitational potential φ and the incremental stress tensor $\boldsymbol{\tau}$ consists of the momentum equation, the Poisson equation and the constitutive relation,

$$\begin{aligned}
\nabla\cdot\boldsymbol{\tau}-\rho_0\nabla\varphi+\nabla\cdot(\rho_0\boldsymbol{u})\nabla\varphi_0-\nabla(\rho_0\nabla\varphi_0\cdot\boldsymbol{u}) &= \rho_0\frac{\partial^2\boldsymbol{u}}{\partial t^2}, && (1)\\
\nabla\cdot(\nabla\varphi+4\pi G\rho_0\boldsymbol{u}) &= 0, && (2)\\
\lambda\nabla\cdot\boldsymbol{u}\boldsymbol{I}+\mu\left[\nabla\boldsymbol{u}+(\nabla\boldsymbol{u})^{\mathrm{T}}\right] &= \boldsymbol{\tau}, && (3)
\end{aligned}$$

where ρ_0 is the reference density and λ and μ are the elastic Lamé parameters, the latter also referred to as the shear modulus. This Lagrangian-Eulerian system of equations can be found in, e.g., Martinec (1984) or Dahlen and Tromp (1998). For the case of spherical symmetry we can decompose the scalar incremental gravitational potential and the displacement vector by means of the scalar spherical harmonic functions $Y_{lm}(\vartheta,\phi)$,

$$\begin{aligned}
\boldsymbol{u}(\boldsymbol{r}) &= u_r(\boldsymbol{r})\boldsymbol{e}_r+u_\vartheta(\boldsymbol{r})\boldsymbol{e}_\vartheta+u_\phi(\boldsymbol{r})\boldsymbol{e}_\phi, && (4)\\
u_r(\boldsymbol{r}) &= \sum_{lm}U_{lm}(r)Y_{lm}(\vartheta,\phi), && (5)\\
u_\vartheta(\boldsymbol{r}) &= \sum_{lm}V_{lm}(r)\frac{\partial Y_{lm}}{\partial\vartheta}(\vartheta,\phi)-W_{lm}(r)\frac{1}{\sin\vartheta}\frac{\partial Y_{lm}}{\partial\phi}(\vartheta,\phi), && (6)\\
u_\phi(\boldsymbol{r}) &= \sum_{lm}V_{lm}(r)\frac{1}{\sin\vartheta}\frac{\partial Y_{lm}}{\partial\phi}(\vartheta,\phi)+W_{lm}(r)\frac{\partial Y_{lm}}{\partial\vartheta}(\vartheta,\phi), && (7)\\
\varphi(\boldsymbol{r}) &= \sum_{lm}F_{lm}(r)Y_{lm}(\vartheta,\phi). && (8)
\end{aligned}$$

The coefficients U_{lm} and V_{lm} create a spheroidal part of displacement and W_{lm} correspond to a toroidal part. We transform (1)–(3) into ordinary differential equations of the second order. For toroidal modes that create neither volume variations nor changes of the gravitational field we have one equation,

$$\mu W''+\left(\frac{2\mu}{r}+\mu'\right)W'-\left(\frac{N\mu}{r}+\mu'\right)\frac{W}{r}=-\rho_0\omega^2W, \qquad (9)$$

where ω is the angular frequency of an individual free oscillation, and for spheroidal modes we obtain a set of three equations,

$$\begin{aligned}
\beta U''+\left(\frac{2\beta}{r}+\beta'\right)U'+\left(\frac{4\rho_0g_0}{r}-4\pi G\rho_0^2-\frac{2\beta+\mu N}{r^2}+\frac{2\lambda'}{r}\right)U-&\\
-(\lambda+\mu)\frac{NV'}{r}+\left(\frac{\lambda+3\mu}{r}-\rho_0g_0-\lambda'\right)\frac{NV}{r}-\rho_0F' &= -\rho_0\omega^2U,\\
\mu V''+\left(\frac{2\mu}{r}+\mu'\right)V'-\left(\frac{\beta}{r}+\mu'\right)\frac{N}{r}V+&\\
+\frac{\lambda+\mu}{r}U'+\left(\frac{2\beta}{r}-\rho_0g_0+\mu'\right)\frac{U}{r}-\frac{\rho_0}{r}F &= -\rho_0\omega^2V,\\
F''+\frac{2}{r}F'-\frac{N}{r^2}F+4\pi G\rho_0\left[U'+\left(\frac{2}{r}+\frac{\rho_0'}{\rho_0}\right)U-\frac{N}{r}V\right] &= 0.
\end{aligned}$$

For the spheroidal modes with $l = 0$, the motion proceeds only in the radial direction and the horizontal displacement vanishes. So, for the radial modes we obtain (10) in a special form,

$$\beta U'' + \left(\frac{2\beta}{r} + \beta'\right) U' + \left(4\rho_0 g_0 - \frac{2\beta}{r} + 2\lambda'\right) \frac{U}{r} = -\rho_0 \omega^2 U. \tag{10}$$

We discretize these equations by highly accurate pseudospectral difference schemes on Chebyshev grids. We thus receive a series of matrix eigenvalue problems for eigenfrequencies and eigenfunctions of the free oscillations. The final eigenvalue problem has a form

$$\left(\mathbf{P}^{-1} \cdot \mathbf{R}\right) \cdot \boldsymbol{Y} = -\frac{1}{\omega^2} \boldsymbol{Y}. \tag{11}$$

where matrices $\mathbf{P}$ and $\mathbf{R}$ depend on the model, vector $\boldsymbol{Y}$ is composed of the eigenfunctions and ω is the angular eigenfrequency.

In order to benchmark our software, we compare our eigenfrequencies and eigenfunctions with those computed by the Mineos software package based on the Runge-Kutta integration techniques as is displayed in Fig. 1. Fig. 2 shows the three-component records of the synthetic acceleration following the 2010 Maule earthquake calculated for the station Pecný (PE: 49.92N, 14.79E), Czech Republic. The acceleration response of a non-rotating anelastic Earth to a step-function moment-tensor source $\mathbf{M}$ situated at $\mathbf{x}_s$ is given at the location of receiver $\mathbf{x}$ by the equation

$$\mathbf{a}(\mathbf{x}, t) = \sum_{n=0}^{\infty} \sum_{l=0}^{\infty} {}_n\mathbf{A}_l(\mathbf{x}) \cos({}_n\omega_l t) \exp\left(-\frac{\omega t}{2Q}\right), \tag{12}$$

where ${}_n\mathbf{A}_l$ is the amplitude of excitation and Q is the quality factor of a mode describing the anelastic dissipation of the compressional and shear energy and the attenuation of the free oscillations. The value of Q can be determined by the equation (cf. Dahlen and Tromp, 1998, eq. 9.54)

$$Q^{-1} = 2\omega^{-1} \int_0^R \left(\kappa K_\kappa Q_\kappa^{-1} + \mu K_\mu Q_\mu^{-1}\right) dr, \tag{13}$$

where $\kappa = \lambda + \frac{2}{3}\mu$ is the incompressibility modulus, $Q_\kappa(r)$ and $Q_\mu(r)$ are the bulk and shear quality factors of the model and the Fréchet kernels K_κ and K_μ depend on the modal frequencies and eigenfunctions.

However, the splitting of free oscillations due to the rotation and associated ellipticity significantly affects the spectra of the gravest modes, so in application on real data we must follow normal-mode perturbation theory by Dahlen and Sailor (1979). Then, the acceleration response of an elliptical Earth model rotating with the sidereal angular velocity Ω at the receiver position $\mathbf{x}$ in time t for an isolated multiplet is

$$\begin{aligned} a(\mathbf{x}, t) \;\; = \;\; & \mathrm{Re} \sum_m \left[1 + m\chi(\Omega\omega_0^{-1}) - \tau(1 - 3m^2 N^{-1})\right] r_m^* s_m \times \\ & \times \exp\left[i\omega_0 \left(1 + a + bm + cm^2 + i(2Q)^{-1}\right) t\right], \end{aligned} \tag{14}$$

where $N = l(l+1)$, ω_0 is the frequency and Q the quality factor of the degenerated multiplet, χ is the Coriolis splitting parameter, a, b and c are splitting parameters and τ is the auxiliary variable. Complex scalars r_m and s_m are related to the displacement evaluated in the receiver and source positions, respectively, for each singlet denoted by m. An asterisk stands for complex conjugation.

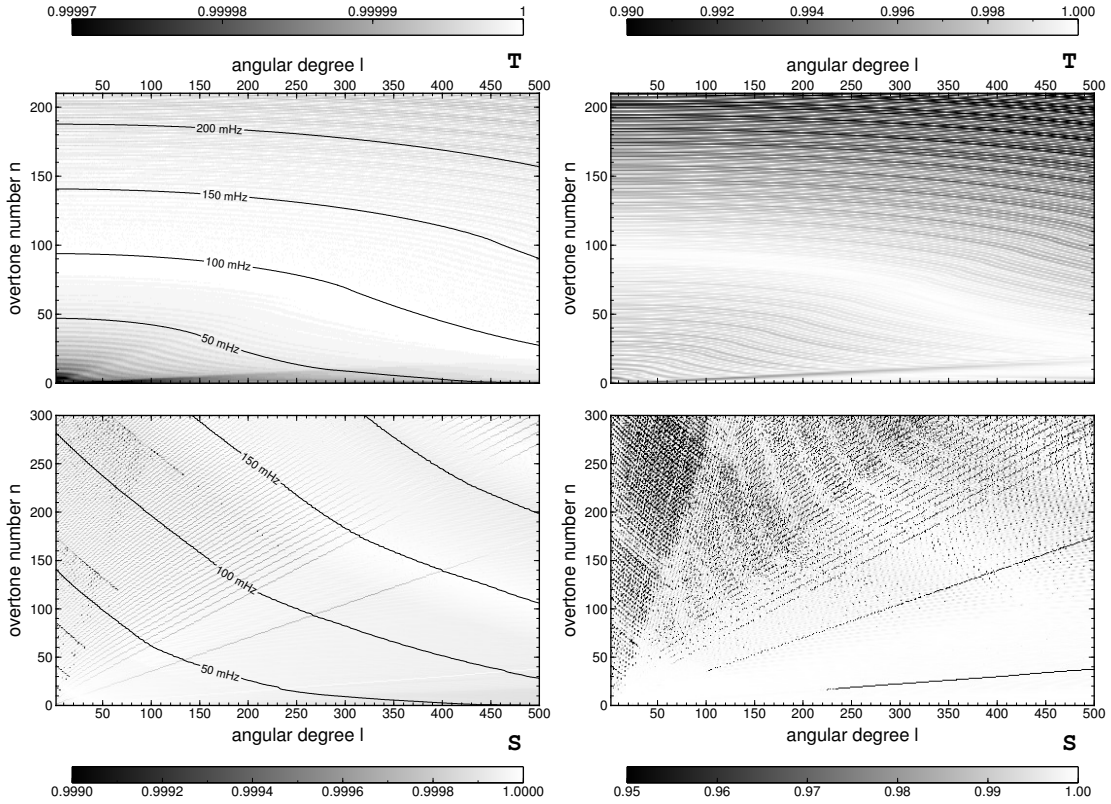

Figure 1: Relative differences between the normal-mode frequencies and quality factors obtained by the Mineos and our matrix-eigenvalue software for the angular degrees up to 500. The upper panel show the toroidal modes and the lower panel show the spheroidal modes.

2 SG records

We summarized the theoretical background needed for computation of the synthetic seismograms generated by point sources. Next, we present its application to low-frequency seismology. We focus on the radial and spheroidal modes in the frequency range up to 1 mHz that affords several advantages by employing the superconducting-gravimeter (SG) data. The SG data are less noisy than seismometer data in this frequency range (e.g., Rosat et al., 2002; Widmer-Schnidrig, 2003; Ferreira et al., 2006; Rosat et. al., 2015), but they provide only the vertical component of oscillations, and the splitting of the low-frequency modes is almost insensible to the 3-D structure of the Earth (e.g., He and Tromp, 1996), so the SG data can be modelled straightforwardly by taking into account multiplet splitting due to only rotation and ellipticity.

The SG data are assembled within the framework of the GGP (http://www.eas.slu.edu/GGP/ggphome.html; Crossley et al., 1999). The geographical distribution of the Global Geodynamics Project (GGP) stations is shown in Fig. 3. The noise-level analysis of these stations was provided by Rosat and Hinderer (2011).

The amplitude spectra of gravity are strongly affected by the solid-Earth tides. The effect of the atmospheric pressure is the second largest; the groundwater-variation influence is an order of magnitude lesser. The standard procedure to remove tides from the recorded data is to subtract the theoretical tidal acceleration from the measured gravity. The most accurate tidal-potential catalogue for high-

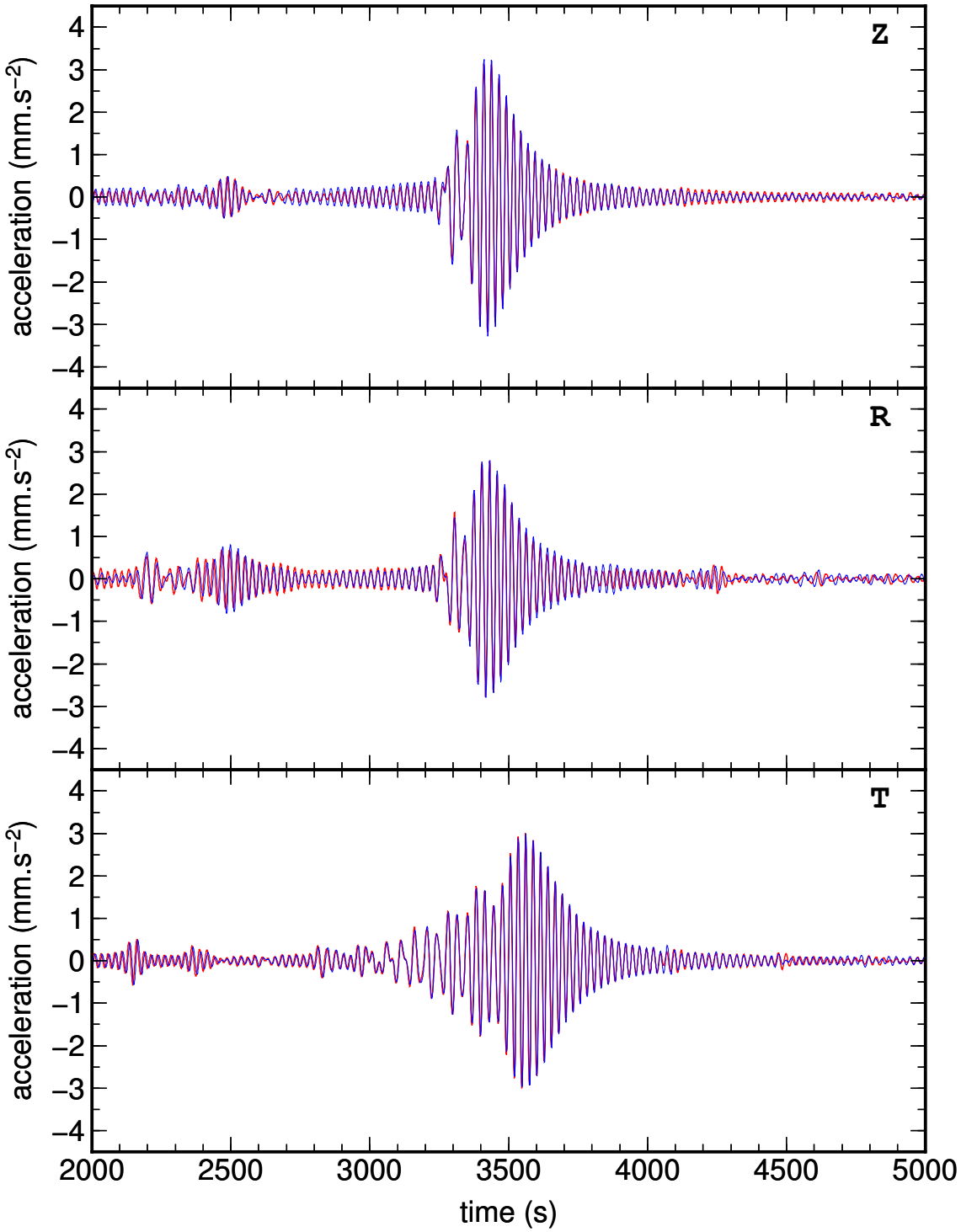

Figure 2: Three components (vertical Z, radial R, transverse T) of synthetic accelerograms for the spheroidal and toroidal modes up to 40 mHz generated by the 2010 Maule earthquake at the station PE. The GCMT source solution was chosen to represent the earthquake. Our accelerograms are plotted in red, those calculated using Mineos in blue. Note that the (Z, R)-components (dominated by the Rayleigh waves) are the sums of the spheroidal modes, whereas the T-component (dominated by the Love waves) is formed of toroidal modes. The zero of the time axis corresponds to the origin time of the earthquake.

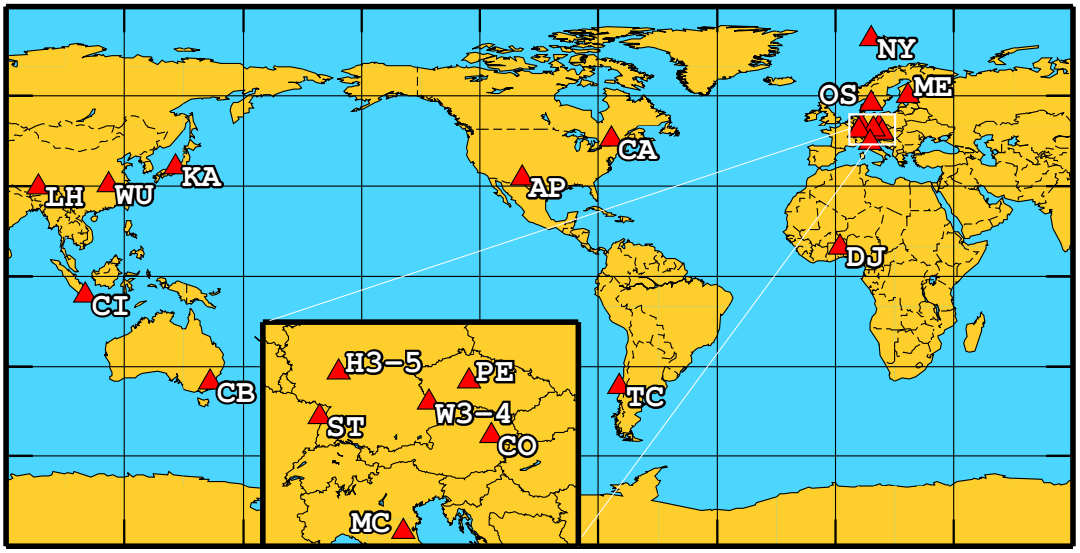

Figure 3: Superconducting gravimeter stations providing free data following the megathrust earthquakes within the Global Geodynamics Project.

precision work is, according to Wenzel (1996a), HW95 described in Hartmann and Wenzel (1995a and 1995b). However, it is sufficient for our purpose to apply a high-pass Butterworth filter with a threshold of 0.1 mHz to remove local tides from the raw gravity data. In this way we also remove most of the tide-joined hydrological effects. We correct the data for the effect of atmospheric pressure with the nominal admittance factor of –3 nm/s^2/hPa. The gravity and atmospheric-pressure data are sampled per 1 second and provided without corrections to disturbances such as spikes, offsets, and other problems. We remove the mean value or linear trend and undersample the data from 1 s to 1 min by standard MATLAB procedures.

The 1952 Kamchatka, 1960 Valdivia (Great Chilean) and 1964 Alaska earthquakes were the strongest earthquakes in the instrumental era before the development of the GGP network of superconducting gravimeters. The GGP subsequently registered the following four megaevents: the 2004 Sumatra-Andaman 2010 Maule, 2011 Tohoku and 2012 Sumatra earthquakes. We focus mainly on the 2010 Maule, 2011 Tohoku-Oki and 2012 Sumatra earthquakes in the following text, since the 2004 Sumatra-Andaman earthquake source process is complicated by an extreme fault-plane length of about 1200 km (e.g., Park et al., 2005; Vigny et al., 2005; Ishii et al., 2005; Banerjee et al., 2005; Braitenberg and Zadro, 2007; de Groot-Hedlin, 2005), and its relatively slow rupture velocity confirmed by many independent studies using various techniques (Krüger and Ohrnberger, 2005; Tolstoy and Bohnenstiehl, 2005; Guilbert et al., 2005; Okal and Stein, 2009; Gahalaut et al., 2010).

In the next chapter we demonstrate the determination of the quality factors of gravest modes as well as the centroid-moment tensor (CMT) of the events from the SG records. We compare our CMT results with those routinely provided by different seismic agencies. We denote the Global Centroid-Moment-Tensor (GCMT) solutions for employed earthquakes as PS1, the U.S. Geological Survey (USGS) solution as PS2 and the W-phase source solution also provided by USGS as PS3. The GCMTs are calculated by summation of Earth normal modes from long-period data provided by the Global Seismographic Network retrieved in a near-real-time network. The USGS uses principally the same method as the GCMT group. The W-phase source

inversion algorithm was specifically developed to handle very large earthquakes like the 2010 Maule and 2011 Tohoku earthquakes. This method exploits the long period content (200–1000 s) of the broadband seismic record preceding the arrival of the surface waves.

3 Results

After the 2010 Maule, 2011 Tohoku and 2012 Sumatra earthquakes the radial and spheroidal modes up to 1 mHz were clearly registered by the Global Geodynamic Project (GGP) network of superconducting gravimeters (SG). Surface acceleration caused by the radial modes depends only on the M_{rr} component of the centroid moment tensor and on its depth assuming its isotropic component to be negligible. Re-evaluation of the modal quality factors Q is needed to obtain constraints on M_{rr} self-consistently. The joint analysis of gravity data from the 2010 Maule and 2011 Tohoku earthquakes yields $Q = 5500 \pm 140$ for the ${}_0S_0$-mode and $Q = 2000 \pm 80$ for the ${}_1S_0$-mode. We were not able to determine the quality factor of the ${}_2S_0$ mode with an accuracy sufficient to allow meaningful constraints ($Q = 1120 \pm 270$). The estimates of Q calculated from the amplitude-spectra decrease for fixed time shifts $\Delta t = 2$ hours are displayed in Fig. 4. Horizontal axes correspond to the shift of the first time window after the origin time. In order to estimate the errors, we calculate the standard deviations of Q from individual station records.

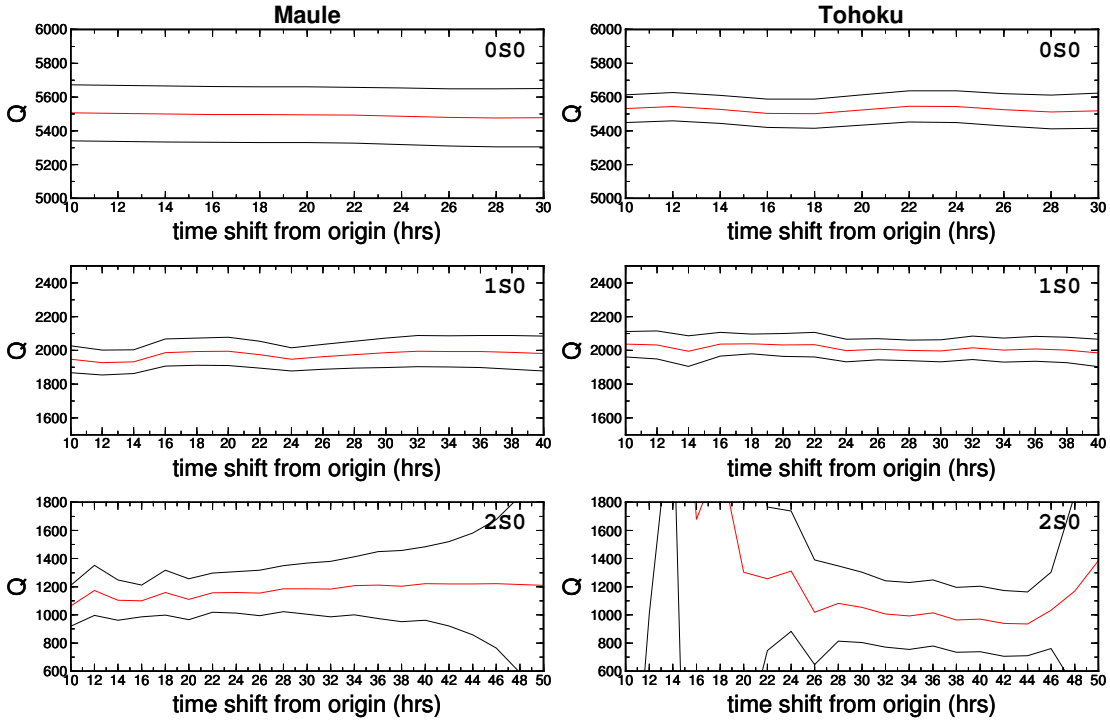

Figure 4: Quality factors of the radial modes estimated from the records after 2010 Maule and the 2011 Tohoku earthquakes from the Fourier amplitude-spectra decrease. Time difference between the windows $\Delta t = 2$ hours was fixed. Horizontal axis shows time shift of the first window after the origin. Red lines denote Q of the radial modes, whereas black lines represent their standard deviations.

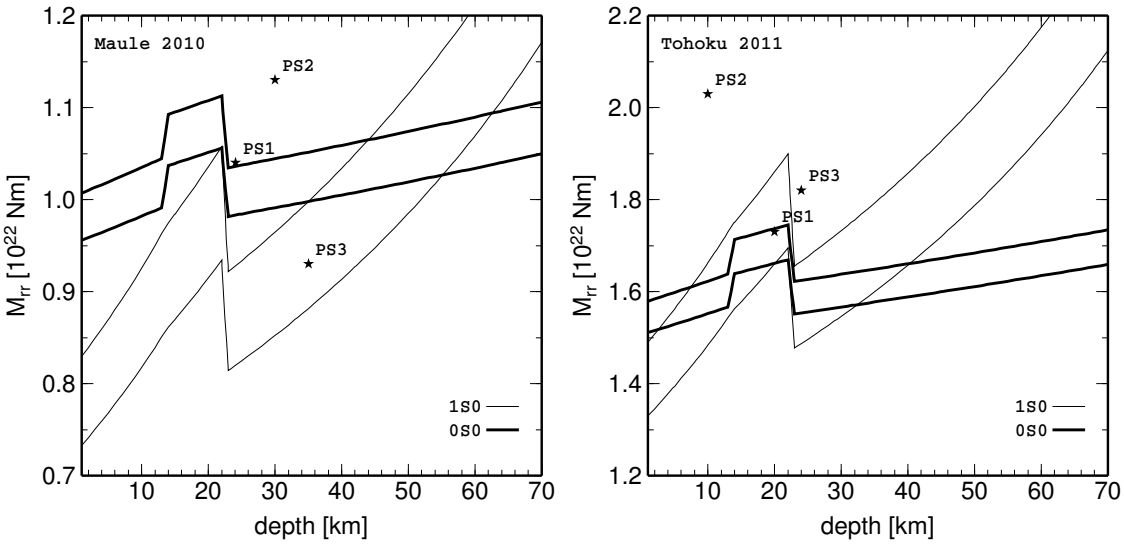

Figure 5: Dependence of the M_{rr} component of the centroid moment tensor on the centroid depth from the ${}_0S_0$ and ${}_1S_0$ amplitudes for the 2010 Maule and 2011 Tohoku earthquakes. For each mode, the interval corresponding to $\pm$ one standard deviation of amplitude-spectra and quality factors is drawn. Stars denote published point-source solutions: Global CMT solutions (Ekström and Nettles, 2010; Nettles et al., 2011) (PS1), USGS CMT solutions (Maule; Tohoku: Polet and Thio, 2011) (PS2), USGS Wphase solutions (Maule; Tohoku: Duputel et al., 2011) (PS3).

The ${}_0S_0$-mode amplitude enables one to obtain a relatively narrow interval of M_{rr} values, whereas ${}_1S_0$-mode amplitude is more sensitive to the centroid depth. We have used these facts to analyze the 2010 Maule $M_w = 8.8$ and 2011 Tohoku $M_w = 9.1$

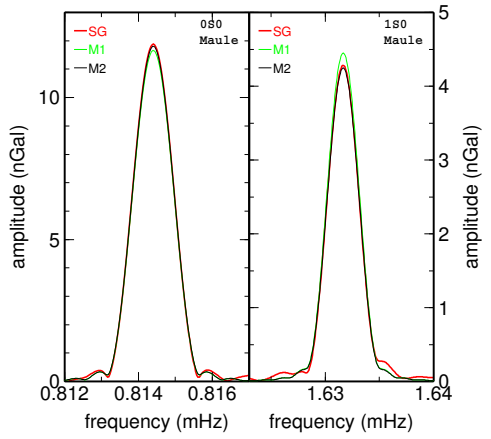

Figure 6: Vertical acceleration amplitude spectra of the modes ${}_0S_0$ and ${}_1S_0$ from the averaged SG data (red) and the two synthetic accelerograms: M1 (green, depth 21 km; $M_{rr} = 1.055 \times 10^{22}$ Nm) and M2 (black, depth 44 km; $M_{rr} = 1.025 \times 10^{22}$ Nm) for the 2010 Maule earthquake. A Hann filter and Fourier transform were applied to 450- (170-)hour time series.

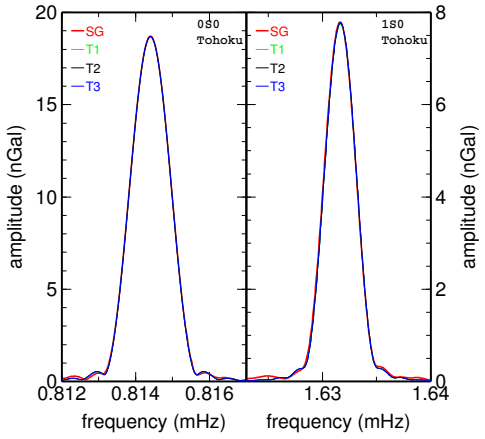

Figure 7: Vertical acceleration amplitude spectra of the modes ${}_0S_0$ and ${}_1S_0$ from the averaged SG data (red) and the three synthetic accelerograms: T1 (green, depth 13 km; $M_{rr} = 1.60 \times 10^{22}$ Nm), T2 (black, depth 18 km; $M_{rr} = 1.69 \times 10^{22}$ Nm) and T3 (blue, depth 29 km; $M_{rr} = 1.60 \times 10^{22}$ Nm) for the 2011 Tohoku earthquake. A Hann filter and Fourier transform were applied to 450- (170-) hour time series.

earthquakes. Superconducting gravimeter data reveal that the M_{rr} components of these earthquakes should be in the interval 0.95–1.15 $\times 10^{22}$ Nm (Maule) and 1.50–1.75 $\times 10^{22}$ Nm (Tohoku), respectively. Fig. 5 demonstrates the constraints on the M_{rr} component of the moment tensor and the depth of the earthquakes obtained from the amplitudes of ${}_0S_0$ and ${}_1S_0$. They are clearly isolated in the spectrum, and the level of observed noise is low (see the mode amplitudes in Figs. 6 and 7), where we demonstrate the agreement in the amplitude spectra between the averaged SG data and the synthetic accelerograms.

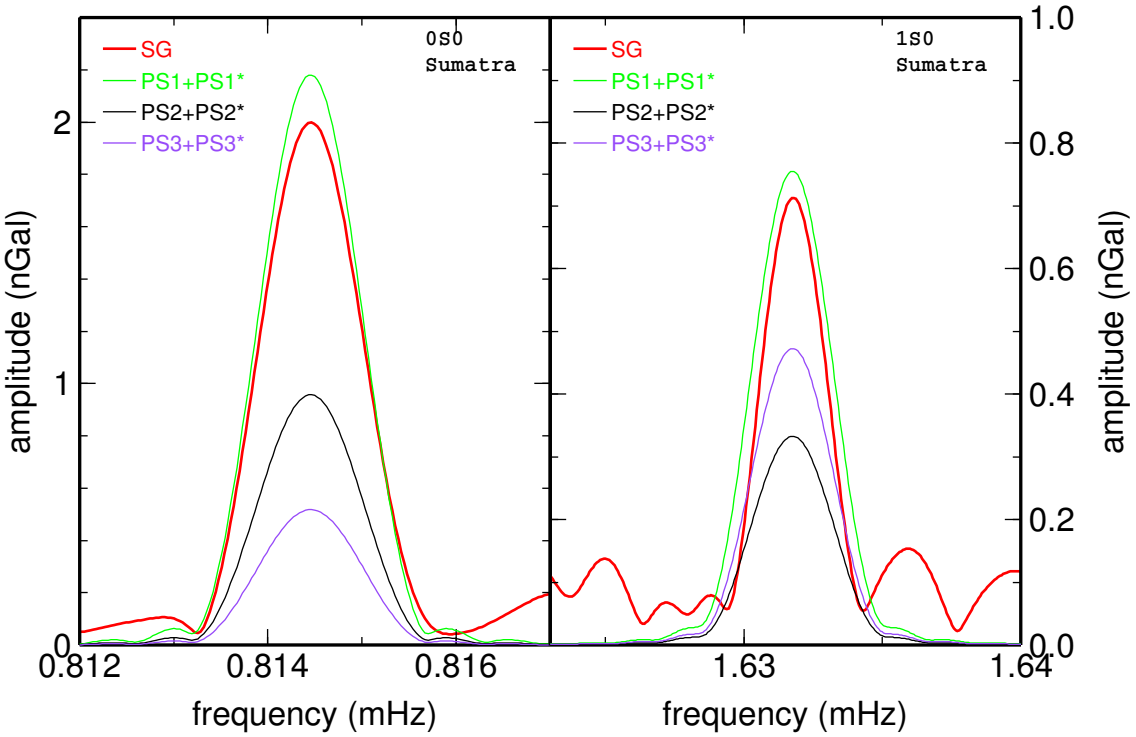

Figure 8: Vertical acceleration amplitude spectra of the modes ${}_0S_0$ and ${}_1S_0$ from the SG data (red - average of three records from Pecný and Wettzell stations) and the three synthetic accelerograms for the agency point-source solutions. A Hann filter and Fourier transform were applied to 450- and 170-hour time series.

The 2012 Sumatra double earthquake consists of two strike-slip events with moment magnitudes higher than 8. Since the fundamental radial mode ${}_0S_0$ has its period of about 20.5 minutes and the second event followed 124 minutes after the main shock, there is approximately a zero phase shift between the fundamental radial oscillations generated by these two events. The same applies for the first radial overtone with the period of about 10.22 minutes. Fig. 8 shows the vertical acceleration amplitude spectra of these two radial modes. The PS3+PS3* solution generates a too weak signal because M_{rr} components of both events are of opposite sign. The PS2+PS2* solution generates weak signal as well; M_{rr} components are of the same sign, but the M_{rr} value of the main shock is too small. We can thus conclude that only the PS1+PS1* solution yields satisfactory fit with the data. These strike-slip earthquakes generated strong horizontal motions; the M_{rr} components generate approximately only 10% of the scalar moment tensor M_0. So, the M_{rr} components are less sensitive than others if the body and surface waves are inverted. However,

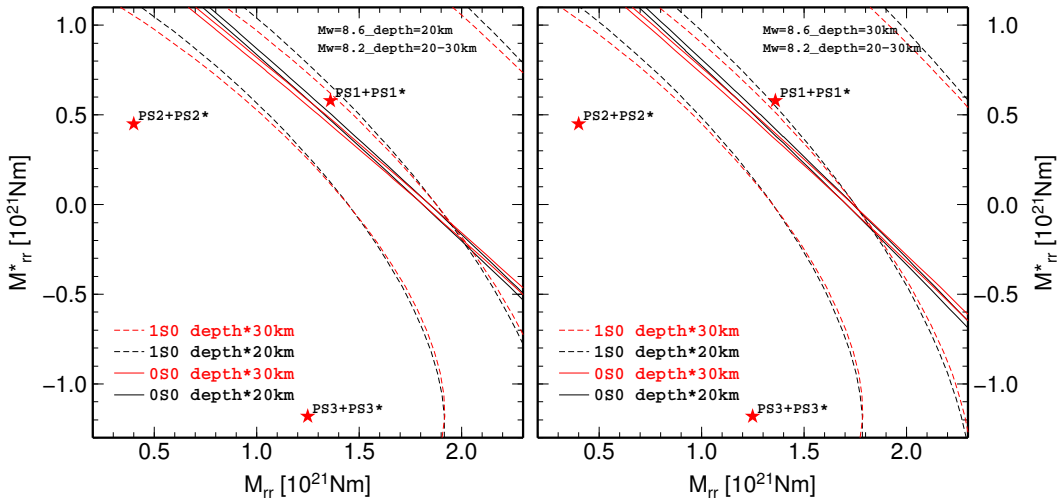

Figure 9: Constraints on the M_{rr} components of the 2012 Sumatra double-event (for several depths of the centroids) obtained from the mode ${}_0S_0$ (solid line) and ${}_1S_0$ (dashed line). For each depth, the interval corresponding to $\pm$ one standard deviation of amplitude spectra obtained from the used records and quality factors is drawn. Stars denote published point-source solutions (PS1, PS2 and PS3).

radial modes are created only by the M_{rr} component and thus they can be used to constrain the M_{rr} components quite well.

The intervals of admissible M_{rr} values for both events are shown in Fig. 9. We fixed the origin times and locations on the values given by PS1 for both earthquakes, since there is no fundamental influence of these quantities on our results. We used the quality factors of radial modes determined from data after the 2010 Maule and 2011 Tohoku earthquakes and inverted the averaged records to find M_{rr} components. We may conclude that M^*_{rr} of the second event cannot be negative and M_{rr} of the main event is smaller than 2×10^{21}Nm. Dependence of the constraints on the studied centroid depths is very weak, as expected. We assume the possible interval of the centroid depths 15–50 km (Duputel et al., 2012). The calculations are presented for the depths of 20 and 30 km. This choice represents the optimal variation of amplitudes, since the amplitudes of the radial modes are sensitive to the shear modulus μ at the centroid depth and our model contains discontinuity at the depth of 22 km (see Fig. 5).

	T [s]	Q_0	Q_1	Q_2	Q_3	$Q_0\,T/2$ [h]
${}_0S_2$	3234	510	496 ± 16	525	477 ± 177	230
${}_0S_3$	2135	417	409 ± 11	380	405 ± 14	124
${}_0S_4$	1546	373	394 ± 27	365	373 ± 9	80
${}_0S_5$	1190	356	350 ± 16	350	364 ± 5	59

Table 1: Periods T of the modes, their quality factors Q used in this study and optimal lengths of the signals according to Dahlen (1982). Q_0 was calculated from the PREM, Q_1 is our estimate contained by averaging over 4 inversion results: inversions started from the Q-values of the PREM and were performed for the centroid depth of 10 and 20 km for the 2010 Maule (20 and 30 km for the 2011 Tohoku) earthquake, Q_2 was estimated by Tanimoto et al. (2012) and Q_3 by Deuss et al. (2013).

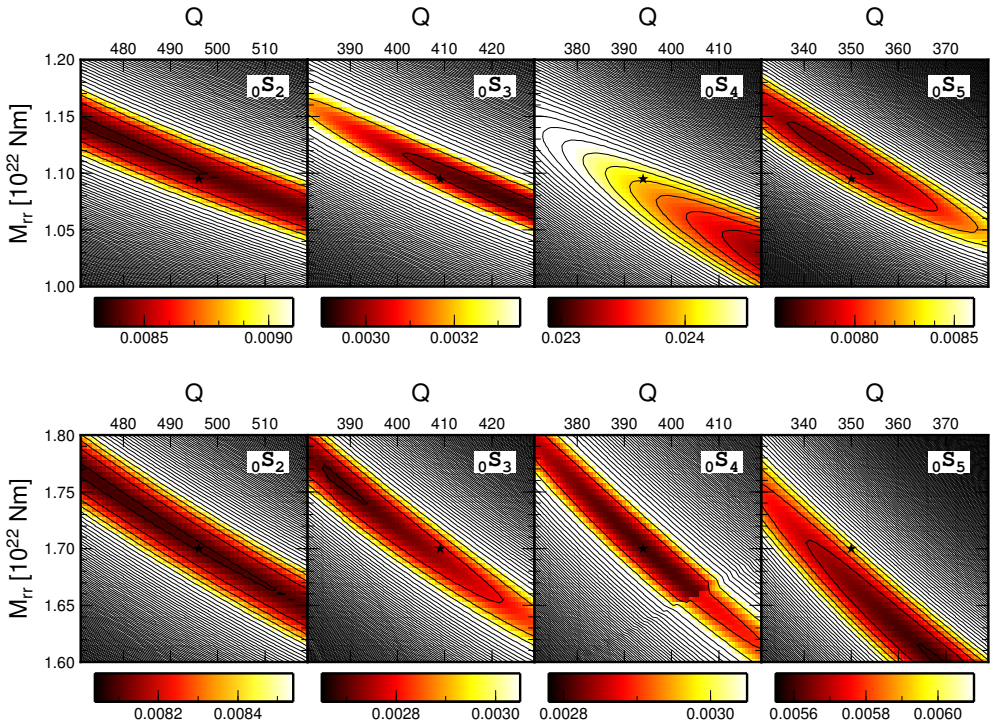

Figure 10: Relative misfits of individual modes for the 2010 Maule (upper panel) and 2011 Tohoku (lower panel) earthquakes for the centroid depth of 20 km showing the trade-off between the M_{rr} component and quality factors of the modes. The stars denote our solutions from the joint inversion. The contour intervals are the same in all panels of a row but the colour scales are different.

The quality factors Q of fundamental spheroidal modal multiplets are also key parameters, and their values used in synthetic calculations can substantially influence the results. The direct determination from their amplitude decrease is difficult, since the modal multiplets consist of several singlets with slightly different frequencies, the descent of the spectral amplitudes is very complicated, thus very long high-quality records are needed. We study the role of their uncertainties in the centroid-moment-tensor (CMT) inversions.

First, we invert the SG data from selected GGP stations to jointly determine the quality factors of these normal modes and the three low-frequency CMT components, M_{rr}, $(M_{\vartheta\vartheta} - M_{\varphi\varphi})/2$ and $M_{\vartheta\varphi}$, that generate the observed SG signal. We use several-days-long records to minimize the trade-off shown in Fig. 10 between the quality factors and the CMT but it is not eliminated completely. We also invert each record separately to get error estimates of the obtained parameters. The employed record lengths and the result quality factors are summarized in Table 1. Obtained quality factors in our inversion procedure are almost independent of changes in the source depth and the choice of the earthquake. In Table 1 we compare our Q values of fundamental modes averaged over performed inversions for both earthquakes with the results obtained by Tanimoto et al. (2012) from cross-correlations in the time domain, by Deuss et al. (2013) performing splitting function inversions, as well as with those from the PREM (Dziewonski and Anderson, 1981). The fundamental-mode-quality factors of the PREM and almost all of Deus et al. (2013) lie within the obtained confidence interval but the results of Tanimoto et al. (2012) differ more.

The highest standard deviation was obtained for the mode ${}_0S_4$ which corresponds to the problems with its fit as demonstrated in Fig. 11. Fig. 11 shows the amplitude spectra of synthetic and measured signals averaged by the time-window lengths to demonstrate data fitting reached in our inversion procedure. We obtained excellent fit for the modes ${}_0S_2$, ${}_0S_3$ and ${}_0S_5$ but worse results for the mode ${}_0S_4$.

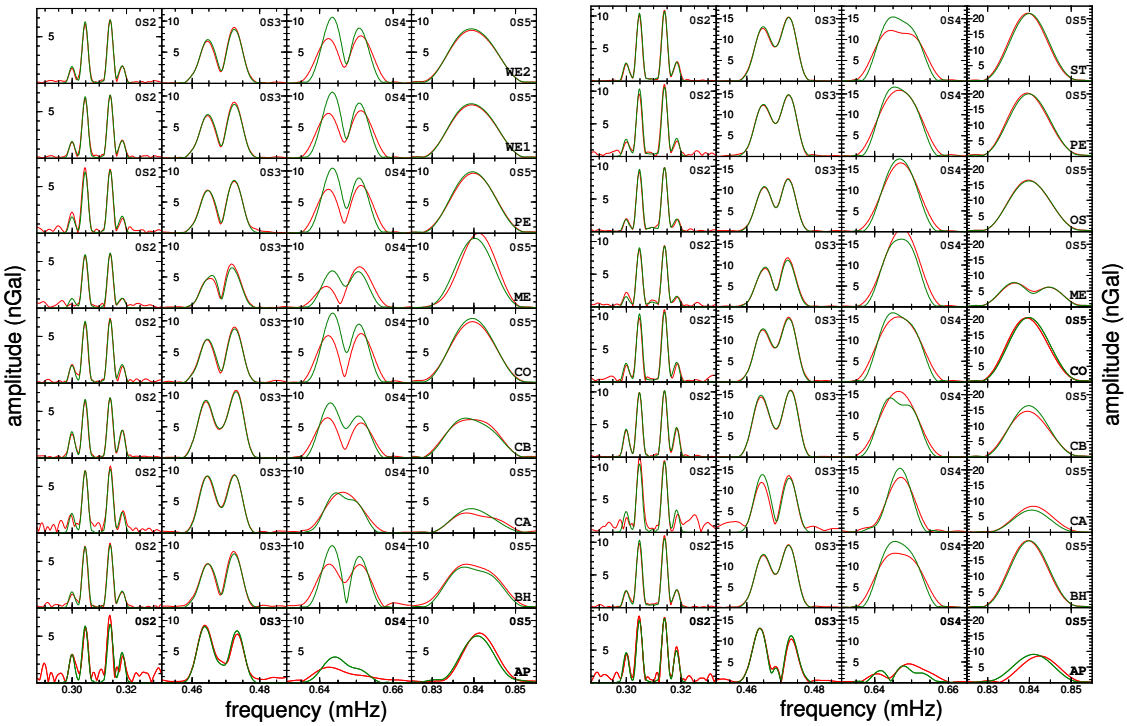

Figure 11: Vertical acceleration amplitude spectra of the studied modes from the SG data (red) and synthetics (green) after the 2010 Maule (left panel) and 2011 Tohoku (right panel) earthquakes. The synthetic signal was calculated for the solution of joint inversion at the depth 20 km (10 km) for the Maule (Tohoku) earthquake. A Hann filter and Fourier transform were applied to the time series of the length shown in the last column of Table 1 starting 2 hrs after the origin times and averaged by the length of the time windows.

Consequently, we employ the GGP records of 60-hrs lengths for several published modal-quality-factor sets and inverted only the same three CMT components. The obtained CMT components shown in Fig. 12 are close to the solution from the joint Q-CMT inversion of longer records and resulting variability of the CMT components is smaller than differences among routine agency solutions. Reliable low-frequency CMT components can thus be obtained for any quality factors from the studied sets. For the 2011 Tohoku earthquake all inversions yield better misfit than the reference Global CMT solution with the PREM Q-values, i.e., the re-evaluation of the CMT components plays a substantial role in the misfit reduction. Moreover, our new re-evaluation of the modal quality factors results in further misfit improvement. However, the misfits for the 2010 Maule earthquake were not improved. The probable reason is that the fit of the mode ${}_0S_4$ in the case of the 2010 Maule earthquake is poor for any choice of the quality factors and most of the misfit is thus created by this mode as shown in Fig. 13 where the amplitude spectra of 60-hrs long synthetic and measured signals averaged by the time-window lengths are displayed.

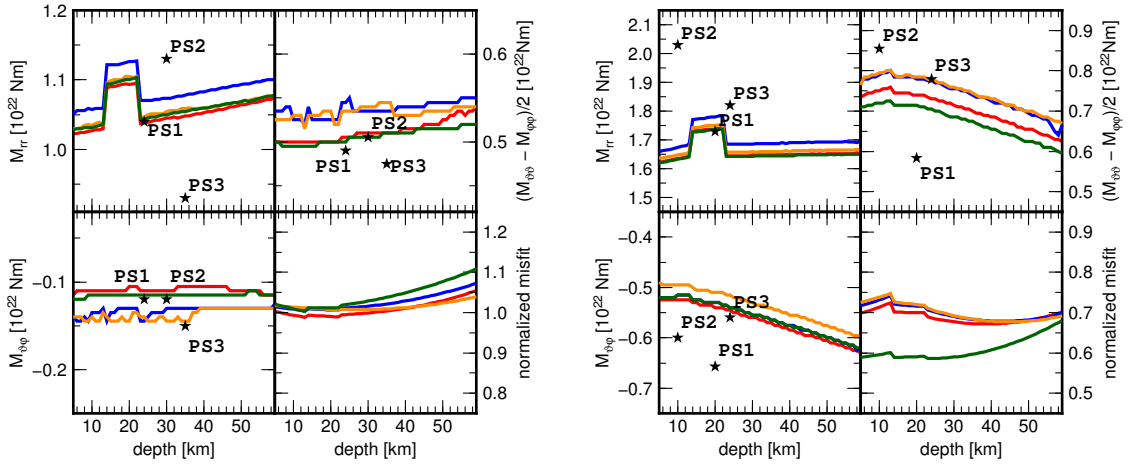

Figure 12: Dependence of the M_{rr}, $(M_{\vartheta\vartheta} - M_{\varphi\varphi})/2$ and $M_{\vartheta\varphi}$ components of the centroid moment tensor on the centroid depth obtained from the inversion of vertical acceleration of the spheroidal modes up to 1 mHz for four sets of Q (red Q_0, green Q_1, blue Q_2, orange Q_3). The left (right) panel is for the 2010 Maule (2011 Tohoku) earthquake. Stars denote published point-source solutions (PS1, PS2 and PS3). The last panel shows the relative misfits of inversions as functions of depth normalized by the misfits of the solution PS1 calculated for the PREM quality factors.

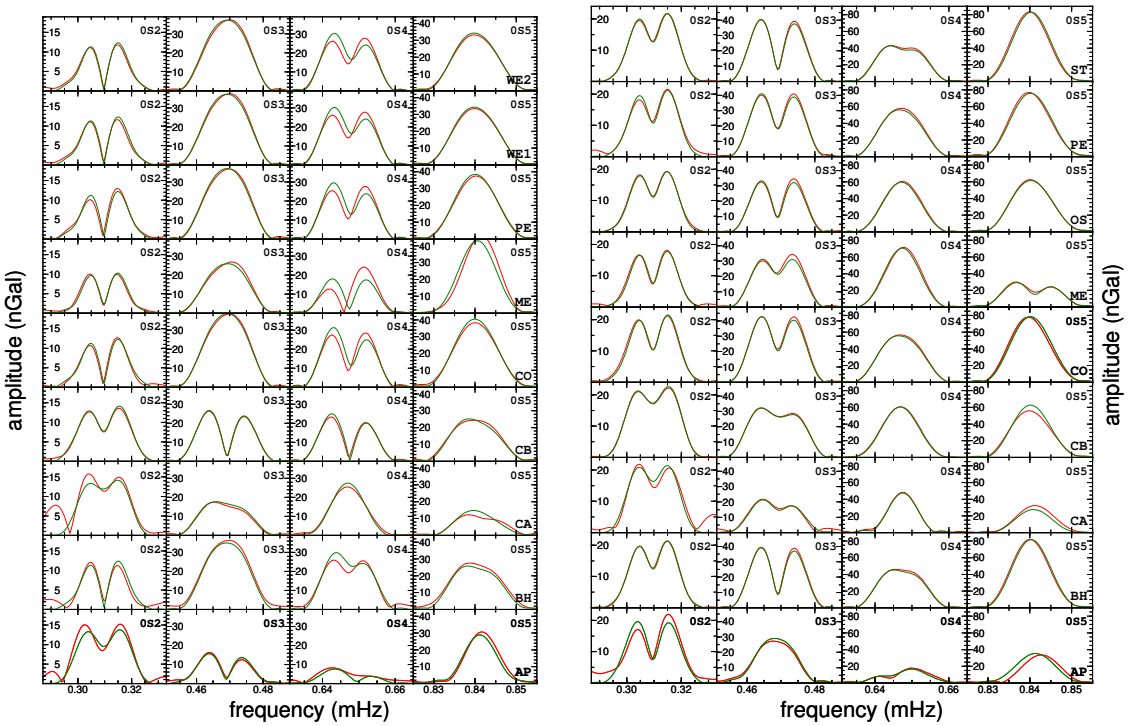

Figure 13: Vertical acceleration amplitude spectra of the studied modes from the SG data (red) and synthetics (green) after the 2010 Maule (left panel) and the 2011 Tohoku (right panel) earthquakes. The synthetic signal was calculated for the optimal CMT solution at the depth 20 km (10 km) for the Maule (Tohoku) earthquake when the quality factors were fixed at the Q_1 values from Table 1. A Hann filter and Fourier transform were applied to the time series of 60-hrs length starting 2 hrs after the origin times and averaged by the length of the time window.

Conclusions

In the methodological part of the thesis we have demonstrated that the system of partial differential equations that describes the free oscillations of the Earth can be decomposed into the ordinary differential equations by spherical harmonic analysis and directly discretized by means of finite-difference schemes with pseudospectral accuracy. The original problem can thus be transformed to a series of matrix eigenvalue problems that can be solved by standard numerical routines. Using numerical libraries for matrix spectral analysis, the eigenfunctions and eigenfrequencies of the fundamental mode and overtones are simultaneously obtained and a high accuracy up to a discretization limit is achieved. Eigenfrequencies and eigenfunctions calculated from these discretized systems agree with those obtained from the classical method, as represented by the Mineos software package based on Runge-Kutta integration techniques.

In this decade, three megathrust events occurred (2010 Maule, 2011 Tohoku, 2012 Sumatra double event) that were also recorded by the network of superconducting gravimeters within the Global Geodynamic Project. We have analyzed their records and showed that the level of noise is sufficiently low for the gravest spheroidal and radial modes. We employed these data to source mechanism inversions to address the question, whether the methods routinely used to estimate centroid-moment-tensor solutions are suitable to get low-frequency limits of the moment tensor.

Since the data are compared with synthetic accelerograms, the knowledge of quality factors is crucial. Surprisingly, there is still rather high uncertainty in the published quality factors. Their direct estimates for the spheroidal modes are complicated due to multiplet splitting which causes rather complex amplitude decrease. For this reason we have decided to perform source inversions simultaneously with quality-factors determination. Although the joint structural and source inversion is, in general, a complicated non-linear problem, the advantage of the inversion in sub-mHz frequency range is a small number of inverted parameters. We have introduced an iterative procedure, where in the first step the quality factors are fixed and the source parameters are determined, whereas in the next step the source mechanism is fixed and quality factors are re-evaluated. This method converges quite fast and yields both the quality factors of the individual modes and the low-frequency estimates of the three moment-tensor components. However, very long records to obtain stable solutions of these joint inversions are needed.

We compared our results with those provided by the three agency solutions. The Harvard GCMT Project preferred solution was obtained using 8.5-hr-long seismograms from about a hundred of stations of the GSN filtered between 300 and 500 s (Nettles et al., 2011). In the GCMT Project approach, the moment tensor and source centroid are estimated by matching observed long-period three-component seismograms to synthetic waveforms calculated by summation of the Earth normal modes. The USGS method used to compute the CMTs is based on the formulas by Dziewonski et al. (1981), and they are also used by the GCMT group, but input waveforms are filtered from 130 to 330 s (Polet and Thio, 2011). The third agency solution is based on the real-time W-phase inversions that exploit the long-period content of the broadband seismic record (200–1000 s) preceding the arrival of the surface waves (Duputel et al., 2011). The best agreement of our results is with the GCMT solution, probably due to the applied lower frequency range. However, the

differences between our results and GCMT solutions are not negligible, which points to the problem of source-solutions robustness in the low-frequency range that was mentioned above.

Special attention was paid to the radial modes, where the inversion is quite simple as these modes are generated by only the M_{rr}-component of the moment tensor and the quality factors of these modes can be directly determined from changes of modal amplitudes with time since there is no splitting. Moreover, dependence of radial-mode amplitudes on geographic position of an observer is very weak and thus the data from different stations can be averaged, which yields robust results obtained from the observations of the ${}_0S_0$ and ${}_1S_0$ modes.

Acknowledgements

My special thanks belong to all nice people at the Department of Geophysics in Prague for the friendly atmosphere. I am grateful to the Research Institute of Geodesy, Topography and Cartography for their support within the Center for Earth Dynamic Research. I would like to express my deepest gratitude to all that provided the gravimetric data through the Global Geodynamic Project. The work was supported by the Grant Agency of the Czech Republic under the project No. 14-04372S.

References

Backus G. and Gilbert F., 1961. The rotational splitting of the free oscillations of the Earth. *Proc. Nat. Acad. Sci.*, **47**, 362–371.

Banerjee P., Pollitz F.F. and Biirgmann R., 2005. The size and duration of the Sumatra- Andaman earthquake from far-field static offsets. *Science*, **308**, 1769–1772.

Braitenberg C. and Zadro M., 2007. Comparative analysis of free oscillations generated by the Sumatra-Andaman Islands 2004 and the Chile 1960 earthquakes. *Bull. Seism. Soc. Am.*, **97**, S6–S17.

Crossley D., Hinderer J., Casula G., Francis O., Hsu H.-T., Imanishi Y., Jentzsch G., Kaarianen J., Merriam J., Meurers B., Neumeyer J., Richter B., Shibuya K., Sato T. and van Dam T., 1999. Network of superconducting gravimeters benefits a number of disciplines. *Eos Trans. AGU*, **80**, 121–126.

Dahlen F.A., 1968. The normal modes of a rotating, elliptical Earth. *Geophys. J. R. Astron. Soc.*, **16**, 329–367.

Dahlen F.A. and Sailor R.V., 1979. Rotational and elliptical splitting of the free oscillations of the Earth. *Geophys. J. R. Astron. Soc.*, **58**, 609–623. doi: 10.1111/j.1365-246X.1979.tb04797.x

Dahlen F.A. and Tromp J., 1998. *Theoretical Global Seismology*. Princeton University Press, Princeton, New Jersey.

de Groot-Hedlin C.D., 2005. Estimation of the rupture length and velocity of the great Sumatra earthquake of December 26, 2004 using hydroacoustic signals. *Geophys. Res. Lett.*, **32**, L11303. doi:10.1029/2005GL022695

Duputel Z., Rivera L., Kanamori H., Hayes G.P., Hirshorn B. and Weinstein S., 2011. Real-time W phase inversion during the 2011 off the Pacific coast of Tohoku earthquake. *Earth Planets Space*, **63**, 535–539.

Dziewonski A.M. and Sailor R.V., 1976. Comments on 'The Correction of Great Circular Surface Wave Phase Velocity Measurements From the Rotation and Ellipticity of the Earth' by F. A. Dahlen *J. Geophys. Res.*, **81**, 4947–4950.

Dziewonski A.M. and Anderson D.L., 1981. Preliminary reference Earth model. *Phys. Earth Planet. Inter.*, **25**, 297–356.

Dziewonski A.M., Chou T.-A. and Woodhouse J.H., 1981. Determination of earthquake source parameters from waveform data for studies of global and regional seismicity. *J. Geophys. Res.*, **86**, 2825–2852.

Ekström, G. and Nettles M., 2010. http://earthquake.usgs.gov/earthquakes/eqinthenews/2010/us2010tfan/neic_tfan_cmt.php

Ferreira A.M.G., d'Oreye N.F., Woodhouse J.H. and Zürn W., 2006. Comparison of fluid tiltmeter data with long-period seismograms: Surface waves and Earth's free oscillations. *J. Geophys. Res.*, bf 111, B11307. doi: 10.1029/2006JB004311

Fornberg B., 1996. *Practical Guide to Pseudospectral Methods*, Cambridge University Press, New York.

Freybourger M., Hinderer J. and Trampert J., 1997. Comparative study of superconducting gravimeters and broadband seismometers STS-1/Z in sub-seismic frequency bands. *Phys. Earth Planet. Inter.*, **101**, 203–217.

Gahalaut V.K., Subrahmanyam C., Kundu B., Catherine J.K. and Ambikapathy A., 2010. Slow rupture in Andaman during 2004 Sumatra-Andaman earthquake: a probable consequence of subduction of 90° E ridge. *Geophys. J. Int.*, **180**, 1181–1186.

Guilbert J., Vergoz J., Schisselé E., Roueff A. and Cansi Y., 2005. Use of hydroacoustic and seismic arrays to observe rupture propagation and source extent of the Mw=9.0 Sumatra earthquake. *Geophys. Res. Lett.*, **32**, L15310. doi:10.1029/2005GL022966.

Hanyk L., Matyska C. and Yuen D.A., 2002. Determination of viscoelastic spectra by matrix eigenvalue analysis, in *Ice Sheets, Sea Level and the Dynamic Earth*, ed. by Mitrovica J.X. and Vermeersen B.L.A., Geodynamics Series, 29, AGU, Washington, pp. 257–273.

Hartmann T. and Wenzel H-G., 1995a. The HW95 tidal potential catalogue. *Geophys. Res. Lett.*, **22**, 24, 3553–3556.

Hartmann T. and Wenzel H-G., 1995b. Catalog HW95 of the tide generating potential. *Bull. Inf. Marées Terrestres*, **123**, 9278–9301.

He X. and Tromp J., 1996. Normal-mode constraints on the structure of the Earth. *J. Geophys. Res.*, **101**, 20053–20082.

Ishii M., Shearer P.M., Houston H. and Vidale J.E., 2005. Extent, duration and speed of the 2004 Sumatra-Andaman earthquake imaged by the Hi-Net array. *Nature*, **435**, 933–936.

Krüger F. and Ohrnberger M., 2005. Spatio-temporal source characteristics of the 26 December 2004 Sumatra earthquake as imaged by teleseismic broadband arrays. *Geophys. Res. Lett.*, **32**, L24312.

Martinec Z., 1984. Free oscillations of the Earth. *Travaux Géophysics*, **591**, 117–263.

Nettles, M., Ekström G. and Koss H.C., 2011. Centroid-moment-tensor analysis of the 2011 off the Pacific coast of Tohoku earthquake and its larger foreshocks and aftershocks. *Earth Planets Space*, **63**, 519–523.

Okal E.A. and Stein S., 2009. Observations of ultra-long period normal modes from the 2004 Sumatra-Andaman earthquake. *Phys. Earth Planet. Inter.*, **175**, 53–62. doi:10.1016/j.pepi.2009.03.002

Park J., Song T.-R.A., Tromp J., Okal E., Stein S., Roult G., Clevede E., Laske G., Kanamori H., Davis P., Berger J., Braitenberg C., van Camp M., Lei X., Sun H., Xu H. and Rosat S., 2005. Earth's free oscillations excited by the 26 December 2004 Sumatra-Andaman earthquake. *Science*, **308**, 1139–1144.

Polet J. and Thio H.K., 2011. Centroid-moment-tensor analysis of the 2011 off the Pacific coast of Tohoku Earthquake and its larger foreshocks and aftershocks. *Earth Planets Space*, **63**, 519–523.

Rosat S., Hinderer J. and Crossley D., 2002. A comparison of the seismic noise levels at various GGP stations. *Bull. Inf. Marées Terrestres*, **135**, 10689–10700.

Rosat S. and Hinderer J., 2011. Noise levels of superconducting gravimeters: Updated comparison and time stability. *Bull. Seism. Soc. Am.*, **101**, 1233–1241. doi: 10.1785/0120100217

Rosat S., Calvo M., Hinderer J., Riccardi U., Arnoso J. and Zürn W, 2015. Comparison of the performances of different spring and superconducting gravimeters and STS-2 seismometer at the Gravimetric Observatory of Strasbourg, France. *Stud. Geophys. Geod.*, **59**, 58–82. doi: 10.1007/s11200-014-0830-5

Tolstoy M. and Bohnenstiehl D.B., 2005. Hydroacoustic constraints on the rupture duration, length, and speed of the great Sumatra-Andaman earthquake. *Seis. Res. Lett.*, **76**, 419–425.

Van Camp M., 1999. Measuring seismic normal modes with the GWR C021 superconducting gravimeter. *Phys. Earth Planet. Inter.*, **116**, 81–92.

Vigny C., Simons W.J.F., Abu S., Bamphenyu R., Satirapod C., Choosakul N., Subarya C., Socquet A., Omar K., Abidin H.Z. and Ambrosius B.A.C., 2005. Insight into the 2004 Sumatra-Andaman earthquake from GPS measurements in southeast Asia. *Nature*, **436**, 201–206.

Wenzel H-G., 1996. Accuracy assessment for tidal potential catalogues. *Bull. Inf. Marées Terrestres*, **124**, 9394–9416.

Widmer-Schnidrig R., 2003. What can superconducting gravimeters contribute to normal-mode seismology? *Bull. Seism. Soc. Am.*, **93**, 1370–1380.

Woodhouse J.H. and Dahlen F.A., 1978. The effect of a general aspherid perturbation on the free oscillations of the Earth. *Geophys. J. R. Astron. Soc.*, **53**, 335–354.

Zábranová E., Hanyk L. and Matyska C., 2009. Matrix pseudospectral method for elastic tides modeling. In: Holota P. (Ed.), *Mission and Passion: Science*. Czech National Committee of Geodesy and Geophysics, Prague, 243–260.

Zábranová E., Matyska C. and Hanyk L., 2012a. Tests of the 2011 Tohoku earthquake source models using free-oscillation data from GOPE. *Stud. Geophys. Geod.*, **56**, 585–594. doi:10.1007/s11200-011-9033-5

Zábranová E., Matyska C., Hanyk L. and Vojtech Pálinkáš, 2012b. Constraints on the centroid moment tensors of the 2010 Maule and 2011 Tohoku earthquakes from radial modes. *Geophys. Res. Lett.*, **39**, L18302. doi:10.1029/2012GL052850

Zábranová E. and Matyska C., 2014. Low-frequency centroid-moment-tensor inversion from superconducting-gravimeter data: The effect of seismic attenuation. *Phys. Earth Planet. Inter.*, **235**, 25–32. doi:10.1016/j.pepi.2014.06.013

Author's publications and citation report

1. Zábranová E. and Matyska C., 2014. Low-frequency centroid-moment-tensor inversion from superconducting-gravimeter data: The effect of seismic attenuation. *Phys. Earth Planet. Inter.*, **235**, 25–32. doi:10.1016/j.pepi.2014.06.013

2. Zábranová E., Matyska C., Hanyk L. and Vojtech Pálinkáš, 2012b. Constraints on the centroid moment tensors of the 2010 Maule and 2011 Tohoku earthquakes from radial modes. *Geophys. Res. Lett.*, **39**, L18302. doi:10.1029/2012GL052850

    - Vaľko M. and Pálinkáš V., 2015. SGNoise - a tool for the ambient noise level analysis at superconducting gravimeter stations. *Stud. Geophys. Geod.*, **59**, 188–199.
    - Bogiatzis P. and Ishii M., 2014. Constraints on the moment tensor of the 2011 Tohoku-Oki earthquake from Earth's free oscillations. *Bull. Seism. Soc. Am.*, **104**, 875–884.
    - Ding H. and Shen W., 2013. Determination of the complex frequencies for the normal modes below 1 mHz after the 2010 Maule and 2011 Tohoku earthquakes. *Annals of Geophysics*, **56**, S0563. doi:10.4401/ag-6400
    - Mitsui Y. and Heki K., 2012. Observation of Earth's free oscillation by dense GPS array: After the 2011 Tohoku megathrust earthquake. *Sci. Rep.*, **2**, 931.

3. Zábranová E., Matyska C. and Hanyk L., 2012a. Tests of the 2011 Tohoku earthquake source models using free-oscillation data from GOPE. *Stud. Geophys. Geod.*, **56**, 585–594. doi:10.1007/s11200-011-9033-5

4. Zábranová E., Hanyk L. and Matyska C., 2009. Matrix pseudospectral method for elastic tides modeling. In: Holota P. (Ed.), *Mission and Passion: Science*. Czech National Committee of Geodesy and Geophysics, Prague, 243–260.